Letter

First-order topological phase transitions and disorder-induced Majorana modes in interacting fermion chains

Shruti Agarwal,[1] Shreekant Gawande,[1] Satoshi Nishimoto,[2,3] Jeroen van den Brink,[2,3] and Sanjeev Kumar[1,3]

[1]*Department of Physical Sciences, Indian Institute of Science Education and Research Mohali, Sector 81, S.A.S. Nagar, Manauli PO 140306, India*

[2]*Department of Physics, Technical University Dresden, 01069 Dresden, Germany*

[3]*Institute for Theoretical Solid State Physics, IFW Dresden, 01069 Dresden, Germany*

(Received 11 April 2022; revised 21 February 2023; accepted 27 February 2023; published 20 March 2023)

Using a combination of the mean-field Bogoliubov–de Gennes approach and the density matrix renormalization group method, we discover first-order topological transitions between topological superconducting and trivial insulating phases in a sawtooth lattice of intersite attractive fermions. The topological characterization of different phases is achieved in terms of winding numbers, Majorana edge modes, and entanglement spectra. By studying the effect of disorder on first-order topological phase transitions, we establish disorder-induced topological phase coexistence as a mechanism for generating a finite density of Majorana particles.

DOI: 10.1103/PhysRevB.107.L121106

Introduction. The discovery of topological insulators marked the beginning of a paradigm shift in our approach to understanding ordering phenomena in condensed matter physics [1–6]. Since then, topological phases have become a recurring theme of research in many fields of quantum as well as classical physics [7–13]. The search for new topological phases is driven not merely by our curiosity to achieve a fundamental understanding but also by the potential for their applications. Topological superconductors are of particular importance as these can host Majorana particles that are considered to be the building blocks of quantum computers [14–19]. Topological phases and phase transitions in noninteracting models can be comprehensively understood in terms of the symmetries of the Hamiltonian [20–23]. On the other hand, a general understanding of topological phases in interacting systems is a challenging theoretical problem [24–28].

Phase separation (PS) is a ubiquitous phenomenon displayed by electronic systems [29–31]. While the inability of an electronic system to exist in a uniform density state appears to be an undesirable feature, PS has proven to be of critical importance in understanding certain aspects of the physics of strongly correlated electron systems [32,33]. Invoking electronic PS is for instance essential for theories of the colossal magnetoresistance effect in manganites [34]. Also, some of the theories applicable in the low-doping regime of the famous cuprate superconductors rely on electronic PS [35–37]. To the best of our knowledge, discussions of the electronic PS between a topological and a trivial phase—henceforth referred to as topological PS (TPS)—are lacking in the literature. TPS has general implications that are independent of the detailed parameter choices of the model.

In this Letter, we report the discovery of first-order topological phase transitions in a lattice model of attractively interacting spinless fermions. Using a combination of density matrix renormalization group (DMRG) and mean-field Bogoliubov–de Gennes (BdG) methods, we find that the model hosts topological superconductor (TSC) and charge-modulated insulator (CMI) phases. Some of the topological and trivial phases are separated by first-order boundaries, leading to TPS. We characterize the topological phases with the help of winding numbers, edge modes, and entanglement spectra. We explicitly demonstrate that in the presence of quenched disorder the TPS leads to a phase coexistence with Majorana modes residing at the boundaries of TSC regions. The TPS-based mechanism for generating a finite density of Majorana modes is qualitatively different from known mechanisms [38–41], and is generic as it is applicable to all discontinuous topological phase transitions.

Spinless fermions on sawtooth lattice. Let us consider spinless fermions with attractive interactions residing on a sawtooth lattice described by the Hamiltonian,

$$\begin{aligned} H = &-t\sum_i (c^\dagger_{i,A}c_{i+1,A} + \text{H.c.}) - t'\sum_i (c^\dagger_{i,A}c_{i,B} + \text{H.c.}) \\ &- t'\sum_i (c^\dagger_{i,B}c_{i+1,A} + \text{H.c.}) - V\sum_i \hat{n}_{i,A}\hat{n}_{i+1,A} \\ &- V'\sum_i (\hat{n}_{i,A}\hat{n}_{i,B} + \hat{n}_{i,B}\hat{n}_{i+1,A}) - \mu\sum_{i,s}\hat{n}_{i,s}. \end{aligned} \tag{1}$$

Here, $c_{i,s}$ ($c^\dagger_{i,s}$) annihilates (creates) an electron at the Bravais site i and sublattice $s \in \{A, B\}$, and $\hat{n}_{i,s}$ is the corresponding number operator. Hopping amplitudes are denoted by t and t', and the corresponding attractive interaction strengths by V and V' (see Fig. 1). We set $t' = 1$ as the basic energy scale, and μ denotes the chemical potential. Note that this elementary interacting model Hamiltonian reduces to a monoatomic Kitaev chain supporting p-wave superconductivity for $t = V = 0$, and the noninteracting limit displays a flat-band dispersion for $t'/t = \sqrt{2}$.

Mean-field phase diagram. In order to obtain the mean-field ground states of the Hamiltonian Eq. (1), we decouple

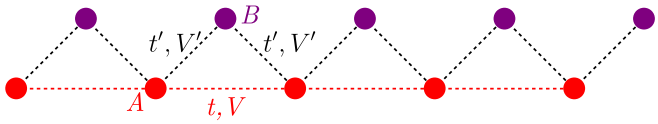

FIG. 1. Schematic representation of the sawtooth lattice model. t, t' indicate the hopping amplitudes and V, V' the attractive interactions between electrons on neighboring sites. Inequivalent sites are labeled A and B.

the interaction term in pairing and density channels [42–45]. This leads to the effective noninteracting Hamiltonian,

$$H = \frac{1}{2}\sum_k \Psi_k^\dagger H_k \Psi_k, \tag{2}$$

with

$$\Psi_k = [c_{k,A}^\dagger \quad c_{k,B}^\dagger \quad c_{-k,A} \quad c_{-k,B}]^\dagger, \quad H_k = \begin{bmatrix} \beta_k & \alpha_k \\ \alpha_k^\dagger & -\beta_{-k}^T \end{bmatrix},$$
$$\beta_k = \begin{bmatrix} -\tilde{\mu}_A - 2t\cos k & -t'(1+e^{-ik}) \\ -t'(1+e^{ik}) & -\tilde{\mu}_B \end{bmatrix},$$
$$\alpha_k = \begin{bmatrix} -2iV\Delta_1 \sin k & -V'\Delta_2(1-e^{-ik}) \\ V'\Delta_2(1-e^{ik}) & 0 \end{bmatrix}, \tag{3}$$

$\tilde{\mu}_A = \mu + 2n_A V + 2n_B V'$, and $\tilde{\mu}_B = \mu + 2n_A V'$. The mean-field parameters $n_{A/B} = \langle \hat{n}_{i,A/B} \rangle$, $\Delta_1 = \langle c_{i+1,A} c_{i,A} \rangle$, and $\Delta_2 = \langle c_{i+1,A} c_{i,B} \rangle = \langle c_{i,B} c_{i,A} \rangle$ are self-consistently determined [42]. Figures 2(a)–2(d) display the variation of different mean-field parameters with chemical potential. The density per site, $n = (n_A + n_B)/2$, varies from 0 to 1, with the end points representing trivial band insulator (BI) phases corresponding to empty or fully filled bands. The pair expectation values Δ_1 and Δ_2 are found to be finite at all nontrivial densities except when there is a plateau at $n = 0.5$ [see Figs. 2(a), 2(c) and 2(d)]. The difference in average densities at two sublattices, $\delta n = n_B - n_A$, remains finite in the entire region. The finite δn is related to the inequivalence of the two sublattices in the noninteracting tight-binding model. Finite values of Δ_1 and Δ_2 identify a superconducting state, within the mean-field description. The $n = 0.5$ plateau regions are characterized by a gap in the single-particle density of states (DOS), together with vanishing pairing amplitudes and finite δn. Therefore, we label these states as charge-modulated insulators (CMIs). We summarize the variations of the mean-field parameters obtained for different values of t in terms of a ground state phase diagram in Fig. 2(e). The topological superconductor (TSC) phases are further labeled as $w = \pm 1$, where w denotes the winding number. Note that the total density displays discontinuities as a function of μ. This is a direct indicator of a first-order phase transition and associated electronic PS in the model. The discontinuities are also present in other mean-field

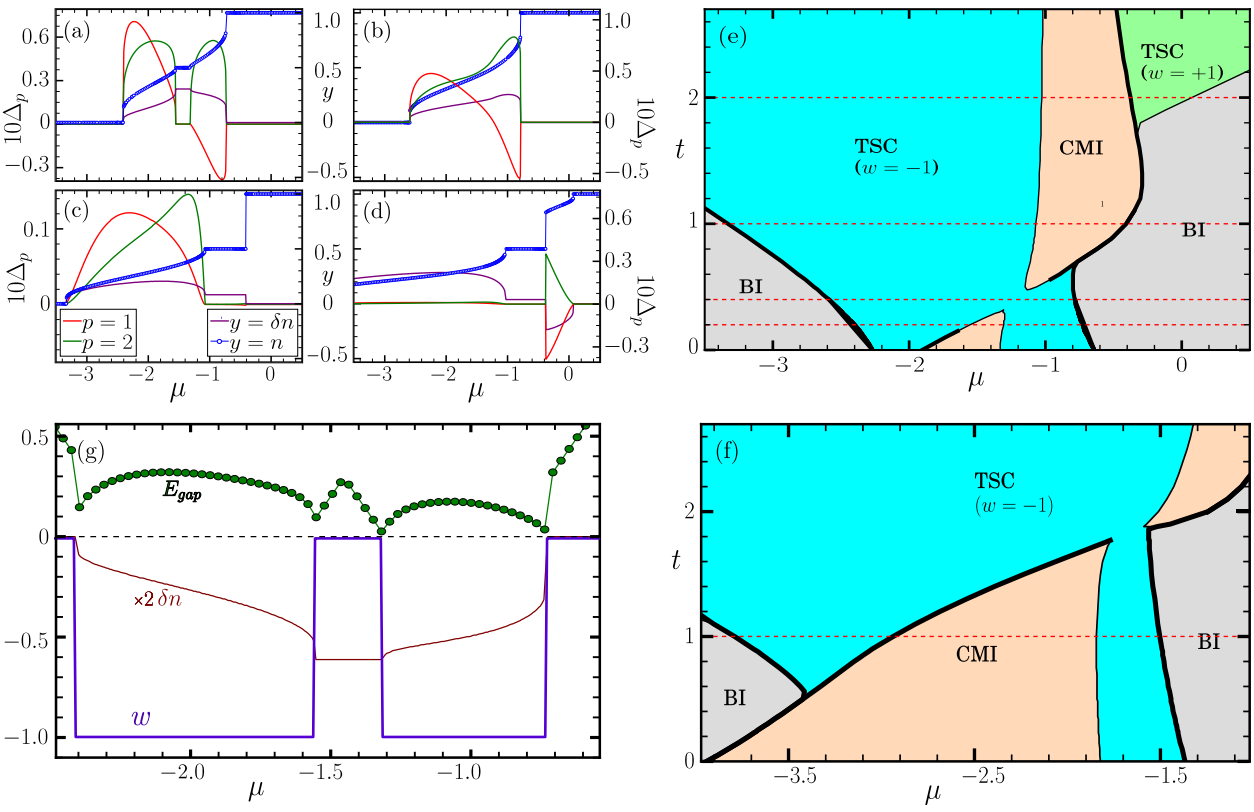

FIG. 2. (a)–(d) Zero-temperature variations of Δ_1, Δ_2, δn, and n with chemical potential for $V = V' = 1$ and for (a) $t = 0.2$, (b) $t = 0.4$, (c) $t = 1.0$, (d) $t = 2.0$. (e) Ground state phase diagram in the t-μ plane constructed from the data similar to that shown in (a)–(d). (f) Same as (e), for $V = 3$ and $V' = 1$. Horizontal dashed lines in (e) indicate the scans for which the data in (a)–(d) are displayed. Dashed lines at $t = 2$ in (e) and at $t = 1$ in (f) also represent the scans for which the DMRG results of Fig. 3 are obtained. (g) Spectral gap, charge modulation, and winding numbers as a function of μ for $t' = V = V' = 1$ and $t = 0.2$.

parameters. While most of the discontinuities seem to involve the trivial BI as one of the states, we also find a robust jump in $n(\mu)$ between the TSC and CMI [see Fig. 2(d)]. The PS locations in μ become extended lines in the phase diagram and are indicated with thick black lines in Fig. 2(e). We perform similar calculations for $V' = 1$ and $V = 3$ and the resulting phase diagram is displayed in Fig. 2(f). The CMI phase occupies a larger region in the phase space and the $w = +1$ TSC is absent. The phase diagram for small V is displayed in the Supplemental Material [42].

Topological characterization. Given that we are dealing with a one-dimensional system, the winding number turns out to be the most natural choice of the invariant that characterizes topologically distinct phases. Using the standard approach to unitarily transform the Hamiltonian into an off-diagonal form [46], we find

$$UH_kU^{-1} = \begin{bmatrix} 0 & \beta_k + \alpha_k \\ (\beta_k + \alpha_k)^\dagger & 0 \end{bmatrix}. \tag{4}$$

The winding number is then defined as [46]

$$w = \frac{1}{2\pi i} \int dk \frac{1}{\det[\beta_k + \alpha_k]} \frac{d}{dk} \det[\beta_k + \alpha_k]. \tag{5}$$

$|w|$ counts how many times $\det[\beta_k + \alpha_k]$ winds around the origin. We find that w takes values $0, \pm 1$ for the Hamiltonian, where $w = 0$ corresponds to topologically trivial phases and a nonzero winding number corresponds to topologically nontrivial phases. Phases with nonzero w are labeled as TSC in the phase diagrams. A representative plot displaying the variation of w with μ is shown in Fig. 2(g). We find that the sign of w is perfectly correlated with the sign of δn, and has an interesting interpretation in terms of the SO(3) theory of intertwined charge and superconducting orders [42,47].

We also compute the quasiparticle spectra for both open as well as periodic boundary conditions. The open boundary spectra display states at exactly zero energy over the μ range corresponding to the superconducting state [42]. We have explicitly checked that these states are Majorana zero-energy modes (MZMs) localized on the edges. In the corresponding periodic boundary spectra, the naive expectation is that the bulk gap must close at the transition point between topologically trivial and nontrivial phases. While the gap seems to reduce, it does not close at the transition point [see Fig. 2(g)]. This seemingly unusual feature is easy to understand if we note that a change in μ does not represent a continuous evolution of the effective noninteracting Hamiltonian in parameter space. This is because the self-consistent values of various mean fields are also parameters of the Hamiltonian which change discontinuously across the transitions.

DMRG results. In order to check the stability of results beyond the mean-field approximation, we perform DMRG calculations for some typical parameter sets. First, the density-density $\langle \hat{n}_{i,s}\hat{n}_{j,s'}\rangle$-$\langle \hat{n}_{i,s}\rangle\langle \hat{n}_{j,s'}\rangle$ and pair-pair $\langle P^\dagger_{ii'ss'}P_{jj'tt'}\rangle$, where $P_{ijss'} = c^\dagger_{i,s}c^\dagger_{j,s'}$, correlation functions are calculated to obtain the ground state phase diagram. The electronic state is characterized by the dominant correlation function with a slower decay as a function of distance. The inverse exponent of the power-law decayed correlation functions ($\propto 1/|i-j|^\gamma$) is plotted as a function of density per site in Figs. 3(a) and 3(b). The resultant phase diagrams, as a function of μ, are also

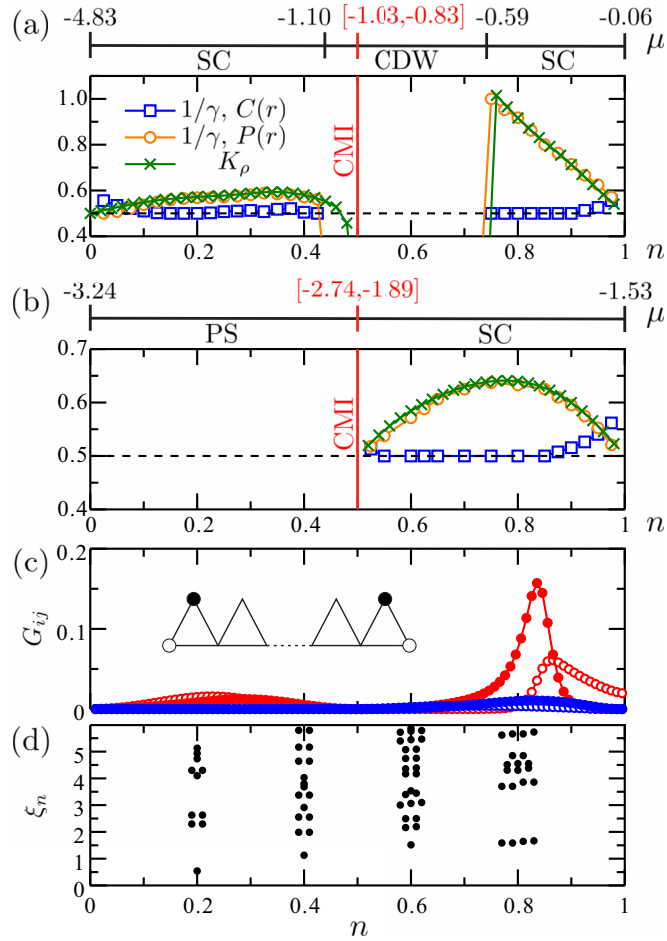

FIG. 3. (a) Inverse exponent of the density-density and pair-pair correlation functions as well as the Tomonaga-Luttinger parameter as a function of density per site for $t = 2.0$ and $t' = V = V' = 1.0$. The corresponding phase diagram is also shown on the top. (b) Plot similar to (a) for $t = t' = V' = 1.0$ and $V = 3.0$. (c) Edge component of the single-particle correlation function for $t = 2.0$, $t' = V = V' = 1.0$ (red) and $t = t' = V' = 1.0$, $V = 3.0$ (blue) with $N = 201$ open cluster. The open and solid circles denote the correlations between edged A sites and between edged B sites, respectively. (d) Entanglement spectra as a function of density per site for $t = 2.0$, $t' = V = V' = 1.0$ with $N = 60$ periodic cluster.

shown. Note that the SC correlation function decays exponentially in the charge density wave (CDW) phase [42,48]. The phase diagrams are further confirmed by the Tomonaga-Luttinger parameter K_ρ, which can be obtained accurately via the derivative of the charge structure factor at $q = 0$ as $K_\rho = \frac{1}{2}\lim_{q\to 0}\langle n(q)n(-q)\rangle$ with $q = 2\pi/N$ and $n(q) = \sum_l (e^{-iql}c^\dagger_{l,A}c_{l,A} + e^{-iq(l+1/2)}c^\dagger_{l,B}c_{l,B})$ [49]. The dominant SC correlation is indicated when $K_\rho > 0.5$. As seen in Fig. 3(a), K_ρ jumps from 0 to ~ 1 at $\mu = -0.59$. This clearly indicates a first-order transition from CDW to topological SC phases at $\mu = -0.59$. It is also confirmed by the divergence of $\partial n/\partial\mu$ at $\mu = -0.59$ [42].

Next, to test the topological nature of the SC phases, the single-particle correlation function $G_{ij} = i\langle \lambda_{i,s}\bar{\lambda}_{j,s'}\rangle$, where $\lambda_{i,s} = c_{i,s} + c^\dagger_{i,s}$ and $\bar{\lambda}_{i,s} = (c_{i,s} - c^\dagger_{i,s})/i$ are Majorana fermion operators, between two ends of open cluster is

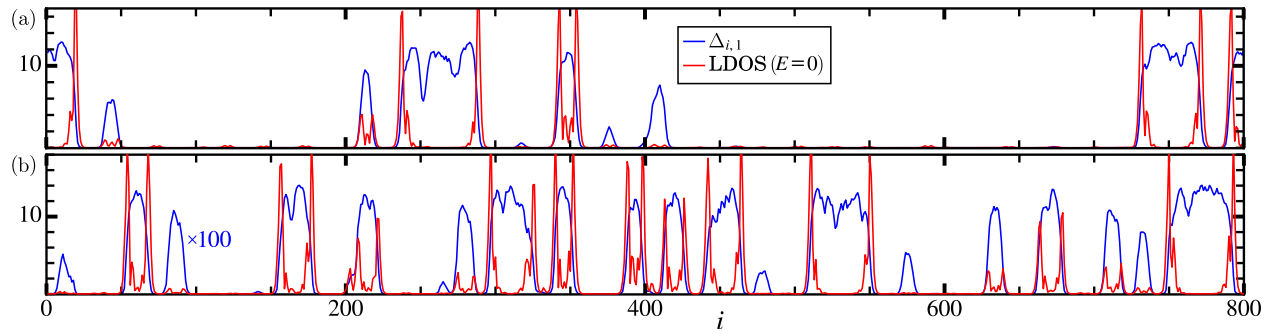

FIG. 4. $\Delta_{i,1}$ and zero-energy LDOS as a function of site index i for (a) $D = 0.4$, $n = 0.46$ and (b) $D = 0.8$, $n = 0.435$. The other parameter values are $V = 3$, $V' = 1$, $t = 1$, $\mu = -2.93$. Note that the $\Delta_{i,1}$ values are scaled up in order to emphasize correlations with the LDOS data.

calculated [50]. In Fig. 3(c) we find a significant enhancement of G_{ij} in the SC phase around $n = 0.8$ for $t = 2.0$ and $t' = V = V' = 1.0$. This indicates that the SC phase is topologically nontrivial. The topological nature is further confirmed by the degeneracy of entanglement spectra (ES) $\xi_n(X = Y)$ using the Schmidt decomposition of the ground state $|\psi\rangle$ as $|\psi\rangle = \sum_\lambda e^{-\xi_\lambda(X)/2} |\lambda\rangle_X |\lambda\rangle_Y$, where $|\lambda\rangle_X$ and $|\lambda\rangle_Y$ are the orthonormal bases for the subregions X and Y, respectively [42,51]. As seen in Fig. 3(d), the lowest level of ES is fourfold degenerate. In a topological phase, the spectrum is expected to be twofold degenerate if the system is cut through a bond [52]. In our system, this corresponds to the entanglement degeneracy as a signature of the zero-energy Majorana edge states. Since two bonds are cut in our calculations of ES because of a periodic chain, the fourfold degeneracy is found in total.

Thus, two of the key features of the mean-field results, the TSC phases and PS, are also confirmed by the DMRG analysis. In contrast to the mean-field results, the DMRG calculations also find a CDW phase and a trivial SC phase [compare Figs. 3(a) and 3(b) with $t = 1$ scans in Figs. 2(e) and 2(f)]. This may be because the instability to trivial PS, as a particle condensation into a self-bound system of concentration, is missing in the mean-field analysis. It is known that the dominance of s-wave conventional SC appears near the trivial PS [53]. Accordingly, a competition between TSC and SC could occur in the DMRG calculations [42].

Topological phase coexistence and Majorana modes. Having discussed the phase diagrams, the important features associated with some of the phases, and their stability beyond mean field, we now focus on the effect of quenched disorder on TPS. We add an on-site disorder term, $\sum_i \epsilon_i(\hat{n}_{i,A} + \hat{n}_{i,B})$, to the Hamiltonian Eq. (1), where $\epsilon_i \in (-D/2, D/2)$ are random variables drawn from a uniform distribution. Since the translational invariance is lost in the presence of disorder, we are forced to perform calculations in real space. The BdG mean-field Hamiltonian in the presence of disorder can be written as

$$H = \tfrac{1}{2}\Psi_r^\dagger H_r \Psi_r + E_0, \tag{6}$$

where the Nambu spinor Ψ_r contains $4N$ components obtained by repeating the index i from 1 to N in

$$\Psi_r = [c_{i,A}^\dagger \quad c_{i,B}^\dagger \quad c_{i,A} \quad c_{i,B} \quad \cdots]^\dagger. \tag{7}$$

H_r is a Hermitian $4N \times 4N$ matrix with nonzero diagonal and off-diagonal 4×4 blocks given by

$$h_{ii} = \begin{bmatrix} \epsilon_i - \tilde{\mu}_{i,A} & -t' & 0 & -V'\Delta_{i,2} \\ -t' & \epsilon_i - \tilde{\mu}_{i,B} & V'\Delta_{i,2} & 0 \\ 0 & V'\Delta_{i,2}^* & -(\epsilon_i - \tilde{\mu}_{i,A}) & t' \\ -V'\Delta_{i,2}^* & 0 & t' & -(\epsilon_i - \tilde{\mu}_{i,B}) \end{bmatrix},$$

$$h_{i,i+1} = \begin{bmatrix} -t & 0 & -V\Delta_{i,1} & 0 \\ -t' & 0 & -V'\Delta_{i,3} & 0 \\ V\Delta_{i,1}^* & 0 & t & 0 \\ V'\Delta_{i,3}^* & 0 & t' & 0 \end{bmatrix} = h_{i+1,i}^*, \tag{8}$$

where $\tilde{\mu}_{i,A} = \mu + V(n_{i-1,A} + n_{i+1,A}) + V'(n_{i-1,B} + n_{i,B})$ and $\tilde{\mu}_{i,B} = \mu + V'(n_{i,A} + n_{i+1,A})$. The above Hamiltonian is diagonalized via real-space Bogoliubov transformations [43–45], and the site-dependent quantum expectation values of density and pairing operators are iteratively computed to obtain self-consistent solutions. We demonstrate the key result by selecting a range of μ values that cover the phase separation between TSC and CMI for $V = 3$, $V' = 1$, and $t = 1$. We display the spatial dependence of the pairing amplitude $\Delta_{i,1}$, along with the local DOS at zero energy, in Fig. 4. Regions with finite pairing amplitudes coexist with regions with zero pairing amplitudes. The number of segments corresponding to the two types of regions increase upon increasing disorder strength [compare Figs. 4(a) and 4(b)]. Most importantly, we find that at the edges of SC regions there exist sharp peaks in the zero-energy local density of states (LDOS). These peaks can only arise from the Majorana zero modes that reside on the edges of all SC segments. It is also clear from the plots that if the length of the SC segment is small, then the two edge modes can hybridize. Our calculations explicitly show that TPS provides an interesting route for generating a finite density of Majorana zero modes. These findings are qualitatively validated by DMRG calculations in the presence of disorder [42]. In fact, the CDW order is strongly suppressed in the presence of disorder [42], and therefore the qualitative agreement between the mean-field and DMRG results is further enhanced.

Conclusion. By investigating a lattice model of attractively interacting fermions, we have unveiled a mechanism for generating a finite density of Majorana particles. The existence of a first-order phase transition and the associated TPS are the key prerequisites for the realization of the proposed mechanism. Within the TPS mechanism, the MZMs can be found

throughout the system in contrast to the conventional mechanism that limits the existence of MZMs only to the edges. Furthermore, given that the on-site potential can be controlled via a suitable application of gate voltages, the MZMs can be mobilized. Given that the implications of our study are general, it is not necessary to have an exact realization of the toy model studied here in order to implement the mechanism in an experimental setup. Nevertheless, for a proof-of-principle verification, the model is realizable in optically trapped ultracold atomic gases [54–56]. Our results also provide a simple understanding of why the conventional idea of a gap closing at topological transitions cannot be generally applicable to interacting systems. Indeed, such scenarios have been reported for interacting quantum spin Hall insulators, in one-dimensional systems and also in Weyl semimetals [57–60]. In general, our study establishes that the interplay of interactions and topology in many-particle quantum systems holds many, possibly useful, surprises.

Acknowledgments. We acknowledge the use of the computing facility at IISER Mohali. We thank Ulrike Nitzsche for technical assistance. This project is funded by the German Research Foundation (DFG) via the projects A05 of the Collaborative Research Center SFB 1143 (Project-ID 247310070) and through the Würzburg-Dresden Cluster of Excellence on Complexity and Topology in Quantum Matter-ct.qmat (Project-ID 390858490-EXC 2147).

[1] C. L. Kane and E. J. Mele, Z_2 Topological Order and the Quantum Spin Hall Effect, Phys. Rev. Lett. **95**, 146802 (2005).
[2] S. Murakami, N. Nagaosa, and S. C. Zhang, Spin-Hall Insulator, Phys. Rev. Lett. **93**, 156804 (2004).
[3] D. N. Sheng, Z. Y. Weng, L. Sheng, and F. D. M. Haldane, Quantum Spin-Hall Effect and Topologically Invariant Chern Numbers, Phys. Rev. Lett. **97**, 036808 (2006).
[4] L. Fu, C. L. Kane, and E. J. Mele, Topological Insulators in Three Dimensions, Phys. Rev. Lett. **98**, 106803 (2007).
[5] C. W. Groth, M. Wimmer, A. R. Akhmerov, J. Tworzydło, and C. W. J. Beenakker, Theory of the Topological Anderson Insulator, Phys. Rev. Lett. **103**, 196805 (2009).
[6] M. Z. Hasan and C. L. Kane, Colloquium: Topological insulators, Rev. Mod. Phys. **82**, 3045 (2010).
[7] V. V. Albert, L. I. Glazman, and L. Jiang, Topological Properties of Linear Circuit Lattices, Phys. Rev. Lett. **114**, 173902 (2015).
[8] J. E. S. Socolar, T. C. Lubensky, and C. L. Kane, Mechanical graphene, New J. Phys. **19**, 025003 (2017).
[9] N. Goldman, J. C. Budich, and P. Zoller, Topological quantum matter with ultracold gases in optical lattices, Nat. Phys. **12**, 639 (2016).
[10] C. L. Kane and T. C. Lubensky, Topological boundary modes in isostatic lattices, Nat. Phys. **10**, 39 (2014).
[11] Z. Yang, Topological Acoustics, Phys. Rev. Lett. **114**, 114301 (2015).
[12] L. Lu, J. D. Joannopoulos, and M. Soljačić, Topological photonics, Nat. Photonics **8**, 821 (2014).
[13] C. H. Lee, S. Imhof, C. Berger, F. Bayer, J. Brehm, L. W. Molenkamp, T. Kiessling, and R. Thomale, Topolectrical circuits, Commun. Phys. **1**, 39 (2018).
[14] K. Flensberg, F. von Oppen, and A. Stern, Engineered platforms for topological superconductivity and Majorana zero modes, Nat. Rev. Mater. **6**, 944 (2021).
[15] X. L. Qi and S. C. Zhang, Topological insulators and superconductors, Rev. Mod. Phys. **83**, 1057 (2011).
[16] C. W. J. Beenakker, Search for Majorana fermions in superconductors, Annu. Rev. Condens. Matter Phys. **4**, 113 (2013).
[17] J. Alicea, Y. Oreg, G. Refael, F. Von Oppen, and M. P. A. Fisher, Non-Abelian statistics and topological quantum information processing in 1D wire networks, Nat. Phys. **7**, 412 (2011).
[18] A. Das, Y. Ronen, Y. Most, Y. Oreg, M. Heiblum, and H. Shtrikman, Zero-bias peaks and splitting in an Al-InAs nanowire topological superconductor as a signature of Majorana fermions, Nat. Phys. **8**, 887 (2012).
[19] C. Nayak, S. H. Simon, A. Stern, M. Freedman, and S. Das Sarma, Non-Abelian anyons and topological quantum computation, Rev. Mod. Phys. **80**, 1083 (2008).
[20] A. Altland and M. R. Zirnbauer, Nonstandard symmetry classes in mesoscopic normal-superconducting hybrid structures, Phys. Rev. B **55**, 1142 (1997).
[21] S. Ryu, A. P. Schnyder, A. Furusaki, and A. W. W. Ludwig, Topological insulators and superconductors: tenfold way and dimensional hierarchy, New J. Phys. **12**, 065010 (2010).
[22] E. Cornfeld and S. Carmeli, Tenfold topology of crystals: Unified classification of crystalline topological insulators and superconductors, Phys. Rev. Res. **3**, 013052 (2021).
[23] Z. Song, C. Fang, and Y. Qi, Real-space recipes for general topological crystalline states, Nat. Commun. **11**, 4197 (2020).
[24] H. Guo and S. Q. Shen, Topological phase in a one-dimensional interacting fermion system, Phys. Rev. B **84**, 195107 (2011).
[25] R. M. Lutchyn and M. P. A. Fisher, Interacting topological phases in multiband nanowires, Phys. Rev. B **84**, 214528 (2011).
[26] E. Tang and X. G. Wen, Interacting One-Dimensional Fermionic Symmetry-Protected Topological Phases, Phys. Rev. Lett. **109**, 096403 (2012).
[27] S. R. Manmana, A. M. Essin, R. M. Noack, and V. Gurarie, Topological invariants and interacting one-dimensional fermionic systems, Phys. Rev. B **86**, 205119 (2012).
[28] M. Ezawa, Exact solutions and topological phase diagram in interacting dimerized Kitaev topological superconductors, Phys. Rev. B **96**, 121105(R) (2017).
[29] R. K. Kremer, A. Simon, E. Sigmund, and V. Hizhnyakov, On the role of electronic and chemical phase separation: Susceptibility and conductivity experiments on $La_{2-x}CuO_{4+\delta}$, in *Phase Separation in Cuprate Superconductors*, edited by E. Sigmund and K. A. Müller (Springer, Berlin, 1994), pp. 66–81.
[30] A. Furrer, J. Mesot, P. Allenspach, U. Staub, F. Fauth, and M. Guillaume, Neutron spectroscopy in $RBa_2Cu_3O_x$ (R = rare earth, $6 \leqslant x \leqslant 7$) compounds: Charge transfer, phase separation, spin fluctuations, in *Phase Separation in Cuprate Superconductors* (Ref. [29]), pp. 101–117.
[31] J. S. Hofmann, E. Berg, and D. Chowdhury, Superconductivity, pseudogap, and phase separation in topological flat bands, Phys. Rev. B **102**, 201112(R) (2020).
[32] D. C. Johnston, F. Borsa, P. C. Canfield, J. H. Cho, F. C. Chou, L. L. Miller, D. R. Torgeson, D. Vaknin, J. Zarestky, J. Ziolo, J. D. Jorgensen, P. G. Radaelli, A. J. Schultz, J. L. Wagner,

S.-W. Cheong, W. R. Bayless, J. E. Schirber, and Z. Fisk, The phase diagrams and doped-hole segregation in $La_2CuO_{4+\delta}$ and $La_{2-x}Sr_xCuO_{4+\delta}$ ($x \leqslant 0.15$, $\delta \leqslant 0.12$), in *Phase Separation in Cuprate Superconductors* (Ref. [29]), pp. 82–100.

[33] V. Hizhnyakov, E. Sigmund, and G. Seibold, Polaron formation and percolative phase separation in HTSC, in *Phase Separation in Cuprate Superconductors* (Ref. [29]), pp. 50–65.

[34] E. Dagotto, *Nanoscale Phase Separation and Colossal Magnetoresistance: The Physics of Manganites and Related Compounds* (Springer, Berlin, 2003), p. 456.

[35] C. Di Castro and M. Grilli, Phase separation as a possible scenario for high T_c superconductors: A particular overview, in *Phase Separation in Cuprate Superconductors* (Ref. [29]), pp. 12–25.

[36] K. I. Kugel, A. L. Rakhmanov, A. O. Sboychakov, N. Poccia, and A. Bianconi, Model for phase separation controlled by doping and the internal chemical pressure in different cuprate superconductors, Phys. Rev. B **78**, 165124 (2008).

[37] E. V. L. de Mello, E. S. Caixeiro, and J. L. González, Theory for high-T_c superconductors considering inhomogeneous charge distribution, Phys. Rev. B **67**, 024502 (2003).

[38] G. E. Volovik, Fermion zero modes on vortices in chiral superconductors, J. Exp. Theor. Phys. Lett. **70**, 609 (1999).

[39] N. Read and D. Green, Paired states of fermions in two dimensions with breaking of parity and time-reversal symmetries and the fractional quantum Hall effect, Phys. Rev. B **61**, 10267 (2000).

[40] J. Alicea and P. Fendley, Topological phases with parafermions: Theory and blueprints, Annu. Rev. Condens. Matter Phys. **7**, 119 (2016).

[41] G. Moore and N. Read, Nonabelions in the fractional quantum Hall effect, Nucl. Phys. B **360**, 362 (1991).

[42] See Supplemental Material at http://link.aps.org/supplemental/10.1103/PhysRevB.107.L121106 for further details of methods and analysis.

[43] J.-X. Zhu, *Bogoliubov–de Gennes Method and Its Applications*, Vol. 924 (Springer, Berlin, 2016).

[44] A. Ghosal, M. Randeria, and N. Trivedi, Role of Spatial Amplitude Fluctuations in Highly Disordered *s*-Wave Superconductors, Phys. Rev. Lett. **81**, 3940 (1998).

[45] A. Ghosal, M. Randeria, and N. Trivedi, Spatial inhomogeneities in disordered *d*-wave superconductors, Phys. Rev. B **63**, 020505(R) (2000).

[46] Y. Gao, T. Zhou, H. Huang, and R. Huang, Majorana zero modes in the hopping-modulated one-dimensional *p*-wave superconducting model, Sci. Rep. **5**, 17049 (2015).

[47] M. Karmakar, G. I. Menon, and R. Ganesh, Vortex-core order and field-driven supersolidity, Phys. Rev. B **96**, 174501 (2017).

[48] S. Ejima, F. Gebhard, S. Nishimoto, and Y. Ohta, Phase diagram of the t-u-V_1-V_2 model at quarter filling, Phys. Rev. B **72**, 033101 (2005).

[49] S. Ejima, F. Gebhard, and S. Nishimoto, Tomonaga-Luttinger parameters for doped Mott insulators, Europhys. Lett. **70**, 492 (2005).

[50] J.-J. Miao, H.-K. Jin, F.-C. Zhang, and Y. Zhou, Majorana zero modes and long range edge correlation in interacting Kitaev chains: analytic solutions and density-matrix-renormalization-group study, Sci. Rep. **8**, 488 (2018).

[51] S.-J. Gu, S.-S. Deng, Y.-Q. Li, and H.-Q. Lin, Entanglement and Quantum Phase Transition in the Extended Hubbard Model, Phys. Rev. Lett. **93**, 086402 (2004).

[52] A. M. Turner, F. Pollmann, and E. Berg, Topological phases of one-dimensional fermions: An entanglement point of view, Phys. Rev. B **83**, 075102 (2011).

[53] E. Dagotto, J. Riera, Y. C. Chen, A. Moreo, A. Nazarenko, F. Alcaraz, and F. Ortolani, Superconductivity near phase separation in models of correlated electrons, Phys. Rev. B **49**, 3548 (1994).

[54] I. Bloch, J. Dalibard, and W. Zwerger, Many-body physics with ultracold gases, Rev. Mod. Phys. **80**, 885 (2008).

[55] A. Bühler, N. Lang, C. V. Kraus, G. Möller, S. D. Huber, and H. P. Büchler, Majorana modes and *p*-wave superfluids for fermionic atoms in optical lattices, Nat. Commun. **5**, 4504 (2014).

[56] T. Zhang and G. B. Jo, One-dimensional sawtooth and zigzag lattices for ultracold atoms, Sci. Rep. **5**, 16044 (2015).

[57] A. Amaricci, J. C. Budich, M. Capone, B. Trauzettel, and G. Sangiovanni, First-Order Character and Observable Signatures of Topological Quantum Phase Transitions, Phys. Rev. Lett. **114**, 185701 (2015).

[58] A. Amaricci, J. C. Budich, M. Capone, B. Trauzettel, and G. Sangiovanni, Strong correlation effects on topological quantum phase transitions in three dimensions, Phys. Rev. B **93**, 235112 (2016).

[59] S. Barbarino, G. Sangiovanni, and J. C. Budich, First-order topological quantum phase transition in a strongly correlated ladder, Phys. Rev. B **99**, 075158 (2019).

[60] L. Crippa, A. Amaricci, N. Wagner, G. Sangiovanni, J. C. Budich, and M. Capone, Nonlocal annihilation of Weyl fermions in correlated systems, Phys. Rev. Res. **2**, 012023(R) (2020).